PERGAMON

Chemical Engineering Science 57 (2002) 1571–1576

Chemical Engineering Science

www.elsevier.com/locate/ces

Membrane reactors for hydrogen production

Ing. Steffen Wieland[a,*], Ing. Thomas Melin[a], Ing. A. Lamm[b]

[a] *Institut für Verfahrenstechnik RWTH Aachen, Turmstr. 46, 52056 Aachen, Germany*
[b] *DaimlerChrysler AG, Forschungszentrum Ulm, Wilhelm-Runge Str. 11, 89013 Ulm, Germany*

Abstract

Fuel cell powered vehicles with on board reforming need compact and lightweight components. A membrane reactor, that combines hydrogen permeable membranes with a methanol steam reformer promises considerable weight and space savings. Its dense metal membranes produce high purity hydrogen over a wide range of pressure and load. The selective removal of hydrogen yields methanol- and CO-conversions that are higher than the equilibrium conversion in a conventional reactor. Results with three different metal membranes in a membrane reactor for steam reforming of methanol are presented. A mathematical model accurately describes the measured performance of the membrane reactor and allows predictions for other values of the process parameters. © 2002 Published by Elsevier Science Ltd.

Keywords: Membrane reactor; Metal membranes; Methanol reforming; Transport processes; Separation; Diffusion

1. General

Although the advantages of membrane reactors (MR) in equilibrium limited reactions such as esterification or dehydrogenation are well documented, they are rarely considered sufficient to justify the added cost of physically integrating reactor and membrane unit. Methanol reforming units for fuel cell cars may well succeed in breaking this rule. In the case of fuel cell powered cars with on board reforming, yield also plays an important role, but there are additional factors that favour a MR. Primarily this is the high-hydrogen purity achievable with dense metal membranes over a wide range of pressure and load. Moreover, a compact and lightweight reactor reduces the thermal mass and improves the turn down ratio.

Technical issues like weight, dynamics, cold start behaviour and parasitic losses are key points for the development. Robust and simple temperature and pressure control systems are highly desirable. The absence of impurities in the fuel cell feed, due to the use of a dense membrane, allows maximum power output at low specific weight and high efficiency. A fuel cell system using a MR combines these features (see Fig. 1).

Fig. 1 displays the schematic of a methanol fuel processor with a MR.

The absence of impurities in the fuel cell entrance due to the use of a dense membrane allows maximum power output at low specific weight and high efficiency. The total efficiency can be improved by using the heat from catalytic combustion of the hydrogen containing off-gas for the endothermic reforming reaction.

2. Methanol steam reforming

Generally there are many ways to produce hydrogen from carbonaceous fuels. However, only methanol allows reforming at moderate temperatures. The endothermic steam reforming of methanol is feasible at temperatures of 200–320°C over a copper zinc catalyst.

To characterize the performance of the reactor we define the catalyst space-velocity B

$$B = \frac{\dot{V}_{H_2}}{V_{kat}}. \quad (1)$$

$\dot{V}_{H_2}$ describes the theoretical hydrogen production at full conversion. Reforming of methanol is generally known as equilibrium limited reaction, which has a conversion rate of over 99%. At high loadings of compact reactors, however, the system becomes kinetically limited which results in a lower conversion rate.

* Corresponding author.
E-mail address: steffen_wieland@lycos.de (Ing. S. Wieland).

0009-2509/02/$ - see front matter © 2002 Published by Elsevier Science Ltd.
PII: S0009-2509(02)00032-5

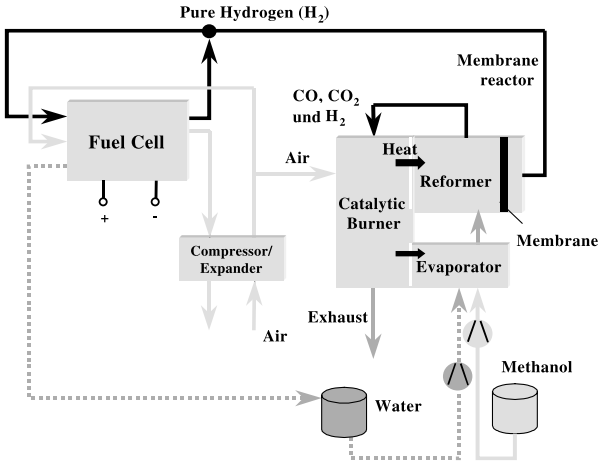

Fig. 1. Schematic of a fuel cell system with a membrane reactor.

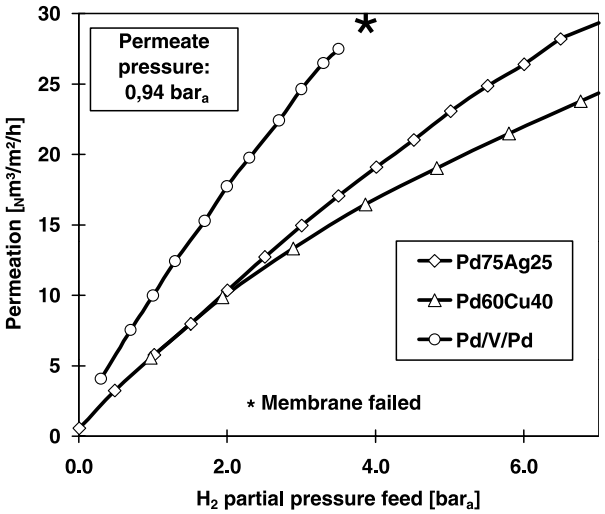

Fig. 2. Rate of permeation of metal membranes.

3. Metal membranes

Large amounts of data on hydrogen permeation through membranes of varying composition have been reported (Shu, 1991). Metal membranes are stable at high temperatures and show a high selectivity towards hydrogen. Investigations of the permeation of pure hydrogen were performed with three different membranes.

Fig. 2 shows the hydrogen permeation rate of the investigated membranes. A coated vanadium membrane of 40 μm thickness had the highest permeation rate. However, this membrane was not stable at partial pressures above 4.2 bar. The $Pd_{60}Cu_{40}$ membrane (25 μm) showed the lowest permeation rate, but was the most stable one and exhibited a much smaller volume expansion than a 25 μm thick $Pd_{75}Ag_{25}$-membrane.

Some of the reactants have a negative influence on the permeation rate of hydrogen through the membrane. Fig. 3 shows the influence of CO at different pressures and temperatures. Compared to pure hydrogen permeation, the flux can decrease by over 70% if the membrane is exposed to CO or methanol. The observed effects suggest that the adsorption of these components on the membrane competes with the adsorption of hydrogen, which is a precondition for hydrogen permeation.

Stationary transport through the membrane can be described using the film model for gas side transport and diffusive transport with constant diffusivity D_M inside the membrane

$$\dot{n}^*_{i,M} = \beta \left(c^{R/F}_{iG} \Big|_{\delta_G} - c^{R/F}_{iG} \Big|_0 \right) = \frac{D_M}{\delta_M} \left(c^{R/F}_{iM} \Big|_0 - c^{P}_{iM} \right) . \quad (2)$$

The concentrations on the membrane can be described by Sievert's law (Sievert, 1929) introducing the partial pressures at the membrane surface and combining all

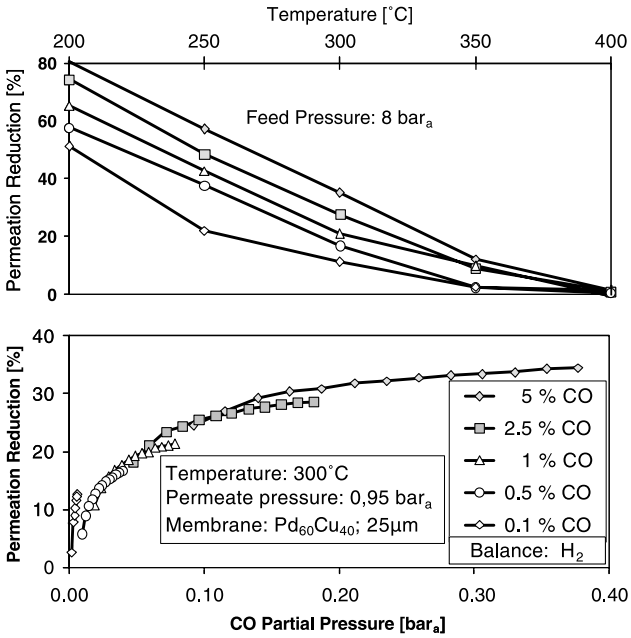

Fig. 3. CO influence on $Pd_{40}Cu_{60}$ membranes.

constants in γ

$$\dot{n}^*_{i,M} = \frac{\beta}{\Re T} \left(p^{R/F}_{iG} \Big|_{\delta_G} - p^{R/F}_{iG} \Big|_0 \right) = \gamma \left(\sqrt{p^{R/F}_{iG} \Big|_0} - \sqrt{p^{P}_{iG}} \right) . \quad (3)$$

Further introducing

$$\Omega = \frac{\gamma \Re T}{\beta} \quad (4)$$

and eliminating the surface concentrations by inserting the two sides of Eq. (3) into one another, yields an expression

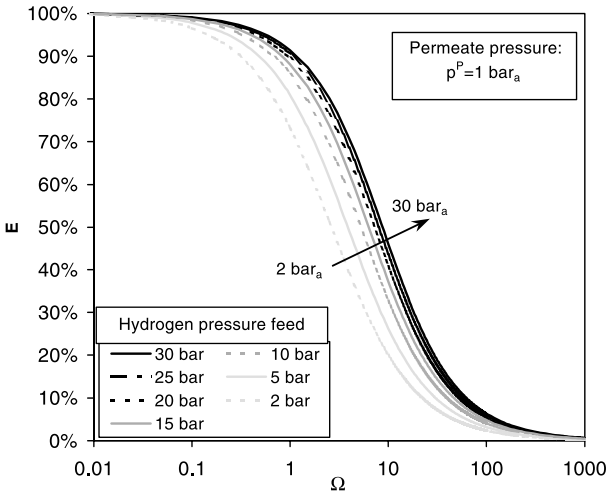

Fig. 4. Ratio of permeation utilization.

Table 1
Calculation of Ω for fuel cell cars

PdCu	PdAg	Pd/V/Pd
0.14–0.063	0.222–0.099	0.347–0.155

containing only bulk concentrations

$$\dot{n}^*_{i,M} = \gamma \left[-\left(\sqrt{p^P_{iG}} + \frac{\Omega}{2} \right) + \sqrt{\left(\sqrt{p^P_{iG}} + \frac{\Omega}{2} \right)^2 - \left(p^P_{iG} - p^{R/F}_{iG}\Big|_{\delta_G} \right)} \right]. \quad (5)$$

Fig. 4 shows the ratio E of the flux given in Eq. (5) divided by the flux at negligible gas side resistance, i.e. for mass transfer coefficient $\beta = \infty$ or $\Omega = 0$. E describes the relative effect of concentration polarisation on total resistance. For $\Omega < 0,1$ mass transfer is limited by diffusion through the membrane. For $\Omega > 0,1$ mass transfer on the feed side becomes limiting.

To determine Ω, β is calculated from literature correlations giving the Sherwood number as a function of the Reynolds and Schmidt numbers.

The correlation is

$$Sh = \frac{\beta \cdot h}{D_G} = aRe^f Sc^g. \quad (6)$$

It should be noted that this correlation is valid only for small to moderate membrane permeability. Otherwise convective flow towards the membrane has to be taken into account. Table 1 shows the calculated values for the investigated membranes over the whole power range of fuel cell cars. Especially for the vanadium membrane concentration polarisation plays a role.

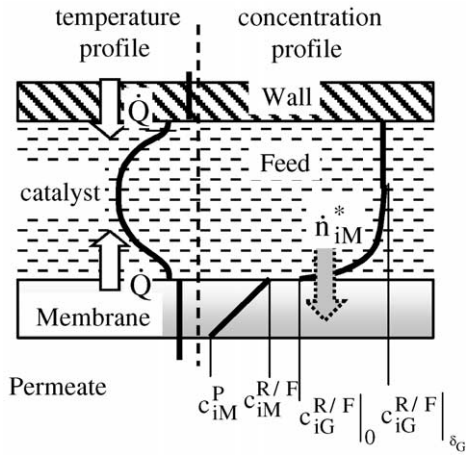

Fig. 5. Schematic concentration and temperature profiles in a membrane reactor.

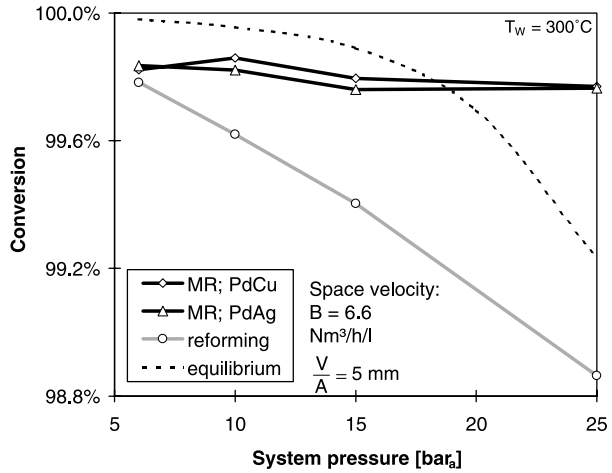

Fig. 6. Conversion as a function of pressure.

4. Membrane reactors

The experimental studies (Wieland, 2000) should demonstrate the technical and practical use of membrane reactors for hydrogen production.

The experiments were performed in a small plate reactor heated electrical from both sides. The height of the catalyst bed could be adjusted between 5.7 and 12 mm by changing the top of the reactor. The temperature was monitored in the middle of the catalyst bed. Pressure, gas flows and compositions were measured at the entrance and exit of the plate reactor. Fig. 5 shows schematically the flow of heat (in), hydrogen (out) and the temperature and hydrogen concentration profiles. The membrane is located only on one side of the plate reactor.

The results in Fig. 6 show that the conversion of a MR exceeds the equilibrium conversion of a conventional reformer if the pressure is increased to 20 bar. Because of the high permeation rate at high pressure, a MR with a PdAg

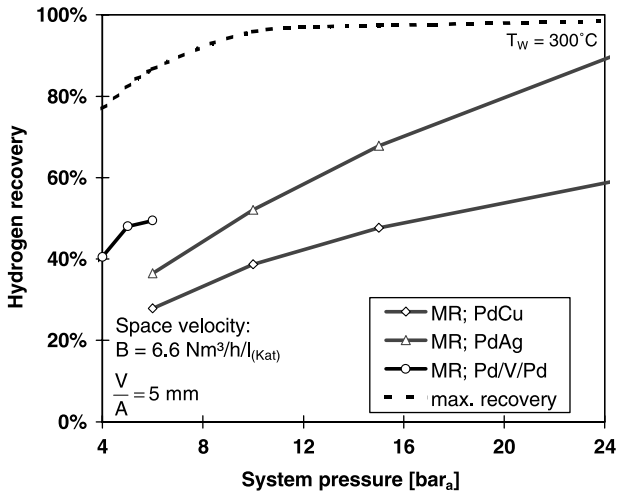

Fig. 7. Hydrogen recovery as function of pressure.

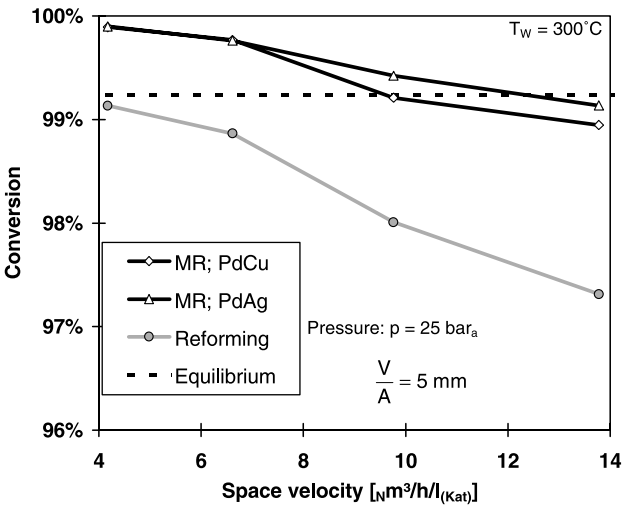

Fig. 8. Conversion as function of space velocity.

membrane almost attains the theoretical maximum of the hydrogen recovery (Fig. 7).

The hydrogen recovery is defined as the ratio of the hydrogen flow in the permeate to the (theoretical) hydrogen flow in the reactor at 100% conversion to H_2 and CO_2:

$$r_{H_2} = \frac{\dot{n}_{H_2,M}}{\dot{n}_{H_2,Rea}} = \frac{\dot{n}^*_{H_2,M}}{3 \cdot B \cdot h}. \quad (7)$$

A comparison including the vanadium membrane could only be made at 6 bar reformat pressure, due to the failure of this membrane at higher pressures. The 40 μm thick vanadium membrane achieved acceptable hydrogen recovery values even at 6 bar.

As weight and volume are key issues in the development, the reactor must also work at high-space velocity. A high turn down ratio without great efficiency loss, e.g. from idle to rated power, is very important for vehicles. A high conversion and hydrogen recovery over the whole power range must therefore be achieved.

Even at very high space velocity, the conversion of the membrane reactor stays at or above the equilibrium of a conventional reformer, as seen in Fig. 8. The conversion of the conventional reformer drops rapidly with increasing space velocity.

At low space velocity the hydrogen recovery in the MR for the PdAg-membrane reaches nearly the theoretical recovery rate (Fig. 9). At high space velocity, by drawing off hydrogen in the membrane reactor, both methanol- and CO-related yield losses are reduced, compared to a conventional reactor.

A further parameter, which influences the performance of the membrane reactor, is the ratio of catalyst volume to membrane area (= bed height).

Fig. 10 shows the effect of a variation of the reactor volume to membrane area ratio. The conversion rate of the MR is always higher than that of a conventional reactor of equal bed height. This effect becomes more pronounced for increased volume to membrane area ratio.

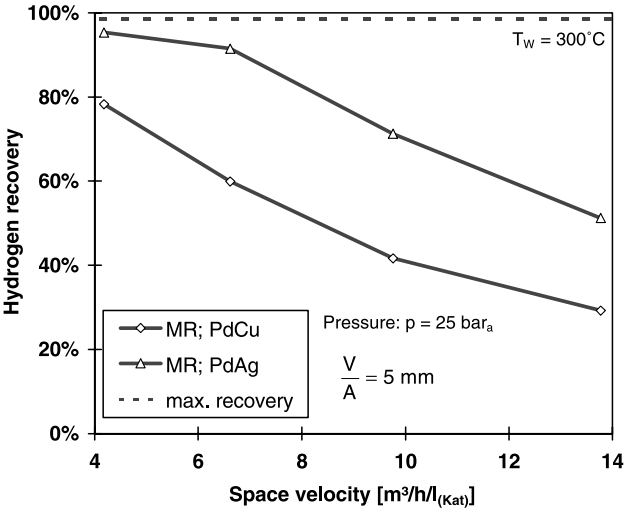

Fig. 9. Hydrogen recovery as function of space velocity.

A high volume to membrane area (e.g. 12 mm membrane reactor in Fig. 9) leads to a drastic drop of conversion when space velocity is increased. This is not caused by the larger mass transfer resistance of the higher bed alone, but also by its poorer heat transfer. The latter effect can also be observed for conventional reforming (5 vs. 12 mm bed height, see Fig. 10).

Methanol reforming is endothermic and increased heat transfer resistance leads to lower temperature in the bed and thus to lower reaction rate.

Fig. 11 shows the conversion if the temperature of the reactor walls is changed from 280°C to 320°C. At all temperatures the conversion of the membrane reactor stays above the equilibrium of the conventional reactor. While at low temperatures the effect of the membrane is higher.

Simulation

The experimental results are compared with those of a stationary one-dimensional membrane reactor model based

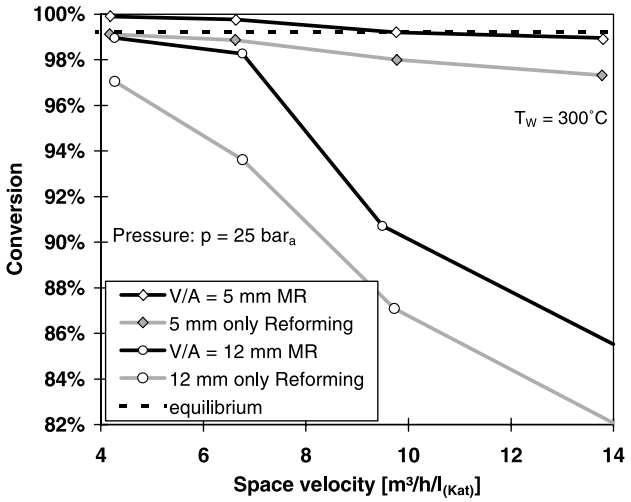

Fig. 10. Conversion as a function of reactor volume to membrane area and space velocity.

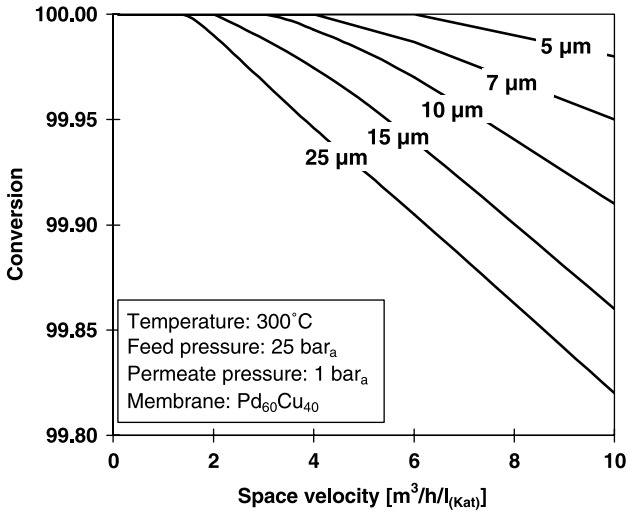

Fig. 12. Conversion rate as a function of space velocity at different membrane thickness.

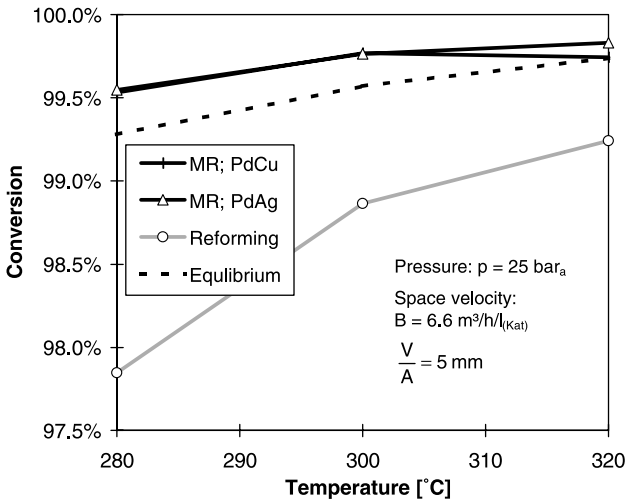

Fig. 11. Conversion as a function of temperature.

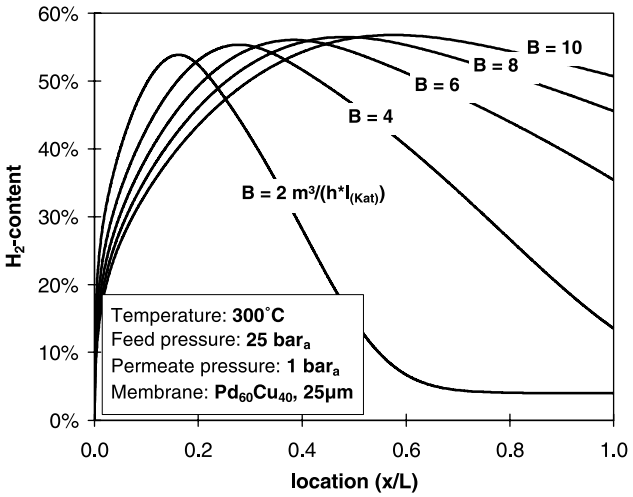

Fig. 13. Hydrogen recovery as a function of the reactor length for different space velocity.

upon adapted literature kinetics (Amphlett et al., 1986), heat and mass transfer correlations and measured membrane permeability data.

The simulation describes the observed temperatures, concentrations and membrane flux data well. It allows system design calculations, parameter variation (e.g. membrane thickness, permeate pressure), data interpolation and—to a certain degree—extrapolation.

Fig. 12 demonstrates the effect of the membrane thickness on the system performance at 25 bar reformer pressure. High conversion and maximum hydrogen recovery can be maintained over the whole range, if sufficiently thin membranes (e.g. 5 µm) are used.

The model also allows for the calculation of gas composition in the reactor along the membrane (see Fig. 13). The hydrogen content rapidly rises to values around 60% and drops towards the exit of the reactor. At low space velocity, the hydrogen partial pressure reaches the permeate pressure after 60% of the reactor length. At higher space velocity, the flux of the relatively thick (25 µm) membrane is no longer sufficient to ensure adequate hydrogen recovery.

5. Conclusions

The future of catalytic membrane reactors for fuel cell cars depends on the availability of membranes that display not only excellent permeate purity, but also high flux at moderate cost and suitable stability in all phases of a typical load cycle.

Furthermore, high membrane permeability would permit a decrease in the system pressure and parasitic losses in the overall system.

A theoretical analysis leads to a coefficient E, which represents the ratio of mass transfer resistance by concentration polarisation to total mass transfer resistance.

The experiments have demonstrated real advantages in yield and recovery with the use of a membrane reactor. It shows a reliable operation in a wide range without delicate temperature and pressure control systems. The weight and space savings it promises are particularly important for fuel cell car applications.

Notation

B	space velocity, $m^3_{(H_2)}/hl_{(Kat)}$
c	concentration, mol/m^3
D_i	diffusion coefficient of component i, m/s^2
H	reactor high, m
L	reactor length, m
$\dot{n}$	molar flow, mol/s
r	recovery rate, %
Re	Reynolds number, dimensionless
Sc	Schmidt number, dimensionless
Sh	Sherwood number, dimensionless
V	volume, m^3
β	mass transfer coefficient, m/s
γ	permeation coefficient, $m^3/hm^2(\text{bar})^n$
δ	layer thickness, m

Indices

G	gas phase
i	component i
Kat	catalyst
M	membrane (surface)
MeOH	methanol
W	wall

Superscripts

$*$	Specific (per area)
P	Permeate side
R/F	Retentate and Feed side

References

Amphlett, J. C., Mann, R. F., & Holland, R. M. (1986). Modeling a catalytic methanol–steam reformer for reactor development and design. *ASME International Energy week* (1996), *conference paper*, 21.1–22.1. New York, pp. 118–124.

Shu, J. (1991). Catalytic palladium based membrane reactors: A review. *Canadian Journal of Chemical Engineering*, *69*, 1036–1060.

Sievert, A. (1929). Aufnahme von Gasen durch Metalle. *Zeitschrift Metallkunde*, *21*, 37–46.

Wieland, S. (2000). Der Membranreaktor als kompaktes Gaserzeugungs— und Gasreinigungssystem für Brennstoffzellen-Antriebe. *VDI Fortschrittsbericht Nr.* 440 *Reihe* 6, VDI–Verlag, Düsseldorf.